# Development of an Operational Hybrid Data Assimilation System at KIAPS

**In-Hyuk Kwon, Hyo-Jong Song, Ji-Hyun Ha, Hyoung-Wook Chun, Jeon-Ho Kang, Sihye Lee, Sujeong Lim, Youngsoon Jo, Hyun-Jun Han, Hanbyeol Jeong, Hui-Nae Kwon, Seoleun Shin, and Tae-Hun Kim**

*Korea Institute of Atmospheric Prediction Systems (KIAPS), Seoul, Korea*

**Abstract:** This study introduces the operational data assimilation (DA) system at the Korea Institute of Atmospheric Prediction Systems (KIAPS) to the numerical weather prediction community. Its development history and performance are addressed with experimental illustrations and the authors' previously published studies. Milestones in skill improvements include the initial operational implementation of three-dimensional variational data assimilation (3DVar), the ingestion of additional satellite observations, and changing the DA scheme to a hybrid four-dimensional ensemble-variational DA using forecasts from an ensemble based on the local ensemble transform Kalman filter (LETKF). In the hybrid system, determining the relative contribution of the ensemble-based covariance to the resultant analysis is crucial, particularly for moisture variables including a variety of horizontal scale spectra. Modifications to the humidity control variable, partial rather than full recentering of the ensemble for humidity further improves moisture analysis, and the inclusion of more radiance observations with higher-level peaking channels have significant impacts on stratosphere temperature and wind performance. Recent update of the operational hybrid DA system relative to the previous 3DVar system is described for detailed improvements with interpretation.

**Key words:** Numerical weather prediction, operational data assimilation, ensemble-variational hybridization, satellite observation assimilation, coupling strategy for hybrid systems

## 1. Introduction

Most numerical weather prediction (NWP) centers have implemented or are pursuing hybrid data assimilation (DA) systems that combine existing variational DA and ensemble forecasts to improve analysis and forecast performance (Kwon et al., 2018). The European Centre for Medium-range Weather Forecasts (ECMWF) employed flow-dependent ensemble forecast error estimations in deterministic four-dimensional variational DA (4DVar) (Bonavita et al., 2016) and the Met Office has modified their global operational 4DVar into a hybrid-4DVar (Clayton et al., 2013) and developed a hybrid four-dimensional ensemble-variation DA (4DEnVar) (Lorenc et al., 2015). The National Centers for Environmental Prediction (NCEP) replaced their operational three-dimensional vari-

ational DA (3DVar) with a 4DEnVar (Kleist and Ide, 2015). Recently, Environment Canada has improved their analysis and forecast accuracy by replacing 4DVar with 4DEnVar for an operational global DA (Buehner et al., 2013; Buehner et al., 2015).

One considerable issue to be resolved in next-generation DA system developments is optimizing the advantages of ensemble-based representations of the background error. Unlike hybrid-4DVar, which uses the ensemble data only at the beginning of the data assimilation window, hybrid-4DEnVar (hereafter H4DEV) makes use of the ensemble trajectories at multiple times within the window. Thus, H4DEV does not require the development or maintenance of tangent linear and adjoint models for a nonlinear NWP model (Song et al., 2009). Considering the continuous evolution of the NWP model's sophistication and the requirements for coupled models that incorporate ocean, sea ice, etc., for the earth simulation framework, and the consequent difficulty of developing and maintaining adjoint models, this gives a clear advantage to H4DEV (Penny and Hamill, 2017).

The Korea Institute of Atmospheric Prediction Systems (KIAPS) was established in 2011 to develop a global NWP model and DA system funded by the Korea Meteorological Administration (KMA) and has developed the Korean Integrated Model (KIM), a non-hydrostatic global model based on a cubed sphere grid. The KIAPS decided to target H4DEV rather than 4DVar for two main reasons:

1. KIM was not completely developed in 2011, so it was impossible to develop tangent linear and adjoint models.
2. We expected that H4DEV could get maximum advantage from the ensemble forecast trajectories with a relatively low computational cost.

As part of the KIM development, we developed 3DVar on the cubed sphere grid and implemented a local ensemble transform Kalman filter (LETKF; Hunt et al., 2007; Shin et al., 2016) as an ensemble DA system that was modified to run within the KIM grid structure. Subsequently, 3DVar and LETKF were combined into an H4DEV (Song et al., 2017c).

The KIM and DA systems have had many updates and significant improvements. KIM recently increased its vertical resolution from 50 to 91 levels and the model upper bound from approximately 60 to 80 km. The upper stratosphere and mesosphere dynamics are key links between short- and

Corresponding Author: Hyo-Jong Song, Korea Institute of Atmospheric Prediction Systems, 4F Park Square, 35 Boramaero 5-gil, Dongjak-gu, Seoul 07071, Korea.
E-mail: hj.song@kiaps.org

🖄 Springer

extended-range weather forecasts and between separate density layers in the atmosphere, hence DA in the upper atmosphere is important to improve forecast performance. As the model top was increased, more radiances with higher peaking channels are available for consideration in the DA. This study introduces the result of sensitivity tests for microwave radiance upper channels.

As the KIM resolution has increased, the accurate representation of humidity, clouds, and other small-scale features have become even more critical. Humidity information should be correctly handled and should incorporate assumed background probability distributions and efficient strategies that consider the DA scheme's relative strengths and weaknesses. The LETKF component of the KIAPS hybrid DA system provides the ensemble initial conditions that can be used for background error covariance (BEC) hybridization. H4DEV improves the moisture field performance through several additional methods that we introduce in this paper.

This study introduces an operationally implemented KIAPS hybrid system that combines Variational DA and LETKF. Critical changes from the 3DVar- to H4DEV-based system are investigated while focusing on analysis quality and attribution as much as possible for each component in the development history. Section 2 describes the operational DA cycling system. The impacts of key changes within the development history are discussed in Section 3; Section 4 discusses the overall outcomes and concludes the paper.

## 2. Data assimilation at the KIAPS

The KIAPS developed 3DVar on the KIM native grid (Song and Kwon, 2015; Song et al., 2017a; Song et al., 2017b), and the system has been operational in semi-real time on KMA's Cray Supercomputer since July 2015. Subsequently, the 3DVar system has been continually and significantly improved with many updates (see Hong et al., 2018, Table A2). The most significant change in the DA system was replacing from 3DVar with H4DEV in February 2017. This section describes how 3DVar was coupled to the KIM and introduces 3DVar in the operational DA system; we also describe the process of replacing 3DVar with H4DEV.

### a. Data assimilation for the Korean Integrated Model

The KIM was developed using the spectral element method (SEM) on a cubed-sphere grid (Choi et al., 2014). A state-of-the-art physics parameterization package was implemented in KIM and demonstrated comparable performance to the KMA Unified Model (UM) in a cold-start test without significant deficiency (Hong et al., 2018). The non-hydrostatic dynamic core included a solver based on the moist flux form of the Euler equations using perturbation from a reference state. The time integration technique of the dynamic core is the explicit time integration scheme of time-split third-order Runge-Kutta (RK3). The KIM employed a finite difference scheme for

vertical discretization in the hybrid sigma pressure coordinate on the Lorenz grid. The vertical hybrid coordinate can be defined with $\eta = [0,1]$ and a weight parameter for the terrain-following coordinate, hence the model levels can be smoothly transformed from terrain-following sigma to pure pressure.

Model variables of KIM are zonal and meridional winds, potential temperature, mixing ratio, and dry surface pressure. The variables that passed to DA are zonal and meridional winds, temperature, mixing ratio and surface pressure rather than dry surface pressure.

These variables are analyzed in DA. In the post processing step, the temperature and surface pressure are converted to potential temperature and dry surface pressure, respectively, to be model variables for the KIM initial condition.

The KIM requires the dry surface pressure because the initial model pressure is calculated from the dry surface pressure using $\eta$. In the post processing step, the dry surface pressure can be calculated by subtracting the moist pressure from the analyzed surface pressure:

$$p_{sfc}^{dry} = p_{sfc}^{anl} - \int_{p_{top}}^{p_{sfc}} q \, dp , \qquad (1)$$

where $p_{sfc}^{dry}$ and $p_{sfc}^{anl}$ are the initial and analyzed dry surface pressure, respectively; $q$ is the specific humidity, i.e. the ratio of water vapor mass to total mass; $p_{top}$ is the pressure at model top; and $p_{sfc}$ the pressure at the surface. The rightmost term in Eq. (1) represents the moist pressure, i.e. the accumulation of moist mass from the model top to bottom.

The interface level pressure is required to calculate the moist pressure, but is not included in the analysis. After calculating the geopotential height using the background pressure, surface height, and virtual temperature, the interface pressure in discretized form is

$$p(\mathrm{k}) = p(\mathrm{k}+1)\exp\left[\frac{g}{R_d \overline{T}_v(\mathrm{k})}(z(\mathrm{k}+1)-z(\mathrm{k}))\right], \qquad (2)$$

where $\mathrm{k} = 1,2,\ldots,K$ indicates the index for vertical levels in which $K$ is the total number of model levels; and $g$, $R_d$, $\overline{T}_v$, and $z$ represent gravity acceleration, the gas constant for dry air, the virtual temperature at the model's level, and the geopotential height at the interface level, respectively.

The pressure in Eq. (2) is a hydrostatic pressure, so the dry surface pressure in Eq. (1) is also in hydrostatic balance. The pressure for each model level is determined by the initial dry surface pressure, thus three-dimensional analysis is vertically re-aligned during the model's initialization. Consequently, the initial condition of non-hydrostatic KIM is in hydrostatic balance, as intended. Cloud liquid water and ice, rain and snow in the background are transferred to the initial condition of KIM during the model initialization.

### b. 3DVar data assimilation in the operational system

We developed the 3DVar system on the native cubed grid by devising a spectral transformation that represents spherical

harmonic functions directly on the cubed-sphere grid (CSG) points without horizontal interpolation (Song and Kwon, 2015). In background error covariance modeling, spectral transformation and Eigen decomposition act as horizontal and vertical filters, respectively. Parameter transformation converts the model variables of zonal wind, meridional wind, temperature, mixing ratio, and surface pressure into control variables of stream function, unbalanced velocity potential, unbalanced temperature, specific humidity, and unbalanced surface pressure. The balanced temperature and surface pressure are related to the rotational wind through a nonlinear balance equation (see Song et al. (2017b) for the control variable transformation details). The static BEC is generated by the NMC method (Parrish and Derber, 1992), which calculates the difference between forecasts starting from two different initial times at the same valid time. Typically, the differences between the 48- and 24-hour forecasts over several months are selected as the background error samples. The NMC method is known to have a lack of correspondence between these 24-hour lagged forecast differences and six-hour forecast errors, so it is necessary to tune the model error variance (Buehner 2005). In the KIAPS DA system, the correspondence between forecast samples and the six-hour forecast error is improved using more diverse pairs of forecasts including shorter lagged forecasts to generate a static BEC. Various forecast differences may represent some background error modes that the 24-hour lagged forecast differences cannot represent. In this study, three pairs: the differences between 48- and 24-hour forecasts, between 36- and 12-hour forecasts, and between 24- and 12-hour forecasts are selected for July-November 2017. First, we removed the bias of each different group by performing sample bias correction and then combined the three groups. In total, 675 samples were used to calculate the static BEC. It was confirmed that the variance of various forecast samples was smaller than that of only 48- and 24-hour forecasts samples, and we found that the BEC calculated using these samples improves the analysis performance in the 3DVar system. The static BEC variances were obtained by rescaling the NMC method variances by factors of 0.7, 0.7, 0.8, 1.0, and 0.7 for stream function, unbalanced velocity potential, unbalanced temperature, specific humidity, and unbalanced surface pressure, respectively. The rescaling factors were determined by comparing the variance of BEC to the background RMSD against IFS analysis.

The KIAPS Package of Observation Processing (KPOP; Kang et al., 2018) has been established to provide quality controlled real-time observations for DA systems (Kang et al., 2018). KPOP obtains Binary Universal Form Representation (BUFR) files for observed meteorological data directly and performs quality control, cloud screening, bias correction, and thinning for conventional and radiance observations. For radiance data assimilation, we have developed an adaptive bias correction (BC) method that calculates the BC coefficients with background at the analysis time rather than using static BC coefficients. The KPOP selects the best observations through the consecutive iterations consisting of BC and the evaluation based on the difference between the observed brightness temperature (TB) and the TB computed from the background state. As seen in Table 1, 3DVar-based system (version 2.5) assimilates Sonde, surface, and aircraft observations, the Advanced Micro Sounding Unit-A (AMSU-A), Microwave Humidity Sounder (MHS) and temperature channels of Advanced Technology Microwave Sounder (ATMS) in microwave radiance observations, the Infrared Atmosphere Sounding Interferometer (IASI) and Cross-track Infrared Sounder (CrIS) in infrared radiance observations, and clear sky radiance (CSR) from COMS satellite. It assimilates the bending angle of Global Positioning System Radio Occultation (GPS-RO) Atmospheric Motion Vector (AMV) and Advanced Scatterometer (ASCAT) in addition. No ATMS moisture channels were assimilated in the 3DVar-based system. We decided not to develop an assimilation module for Atmospheric Infrared Sounder (AIRS) because it has already exceeded its expected lifetime. To assimilate the satellite brightness temperature in 3DVar, the KPOP provides the Jacobian appropriate for the background using the observation operators, where the radiative transfer for the television and infrared observation satellite operational vertical sounder (RTTOV) version 10.2 (Bormann et al., 2011; Hocking et al., 2012) and the radio occultation processing package (ROPP, Culverwell et al., 2015) version 8 are implemented for satellite radiance and GPS-RO observations, respectively.

### c. Replacing 3DVar with H4DEV

Before describing H4DEV, we should introduce the LETKF implementation at KIAPS. While 3DVar was being developed, LETKF was implemented for the ensemble DA system at KIAPS and has been continually updated. The ensemble size of current KIAPS-LETKF is 50 members, and the horizontal resolution of the ensemble model is 50 km. It assimilates most observations assimilated in 3DVar but does not assimilate surface and TC bogus observations. In the first DA cycle, the initial conditions for the ensemble forecasts are produced by adding lagged forecast difference samples from set used to generate for the static BEC to a reconfigured analysis from KMA's installation of the Unified Model (UM) global NWP system. First, we randomly select 50 samples from 225 samples with 48- and 24-hour forecasts differences, and then performed sample bias correction to generate 50 perturbations with an ensemble mean of zero. Second, the 50 perturbations are added to the UM analysis to be the initial condition. It was found that the initial perturbations gave sufficient large spread and approximately Gaussian distributions. LETKF was also run in semi-real time during summer 2016, but we found that the performance degraded as the DA cycle progressed. It was found that this was due to filter divergence caused by reduction of ensemble spread with time evolution. Adaptive multiplicative inflation (Miyoshi, 2011) was already implemented in the LETKF but is was insufficient to inflate the ensemble

**Table 1.** Summary of the difference between the 3DVar and 4DEnVar systems.

| | 3DVar-based system (version 2.5) | H4DEV-based system (version 3.1) |
|---|---|---|
| Background-error covariance | Static background-error covariance generated by the NMC method | Static background-error covariance generated by the NMC method<br>Ensemble background error samples from LETKF |
| Minimization | Single outer-loop; the maximum iteration count is 90 | Multi-resolution multi outer-loop;<br>Four outer-loops with respective total wavenumbers of 42, 85, 170, and 170<br>The alpha control variable appears from the third loop |
| Recentering | None | The ensemble mean of LETKF analyses for u, v, T are recentered to deterministic analyses.<br>Partial recentering for humidity (50% recentered) |
| First guess | Only six-hour forecast at the analysis time<br>Single time bin for observation within the analysis window | Hourly first guess at appropriate time (FGAT)<br>Hourly time bin for observations (seven time bin within the analysis window) |
| Observations | Sonde (u, v, T, q), Surface (u, v, T, q, ps), Aircraft (u, v, T), GPS-RO, AMV, AMSU-A (6), ATMS temperature channels (6), IASI (112), CrIS (60), CSR (1) from COMS, and ASCAT | Adding LEOGEO AMV, ATMS water vapor channels (3) and AMSU-A channels 11,12,13, and 14 (4) |
| Humidity control variable | Specific humidity | Pseudo-relative humidity |
| Innovation QC | No innovation QC in the Var system | Innovation QC for every outer-loop |
| Observation operator | RTTOV and ROPP are not in the Var system, and the Jacobian calculated from the KPOP is used | RTTOV and ROPP are included, so the Jacobian is calculated using updated guesses every outer-loop |
| Tropical cyclone initialization | No TC initialization | TC bogusing using the minimum pressure information for the RSMC Tokyo |
| KIM Model | KIM version 2.5<br>Horizontal resolution: 25 km<br>Vertical resolution: 50 levels with 60 km model top | KIM version 3.1<br>Horizontal resolution: 12 km<br>Vertical resolution: 91 levels with 80 km model top |

● The number in parentheses is the number of channels to be assimilated

spread when satellite radiance observations were assimilated. We additionally implemented an additive inflation to solve the problem (Shin et al., 2018). In the current version of DA system, perturbations for the additive inflation are randomly selected from the 675 forecast difference samples that have been previously generated for the static BEC. The perturbations are added to each ensemble initial state after scaling by a factor of 0.3.

Subsequently, 3DVar and LETKF were combined to build H4DEV (Song et al., 2017c), which replaced semi-real time 3DVar. Introducing ensemble trajectories, which conform the thermodynamic energy, dynamical momentum, and mass conservations that underlie the equation set of the forecast model, into the 3DVar cost function using the ensemble control variable (Lorenc, 2003; Lorenc et al., 2015; Kleist and Ide, 2015; Song et al., 2017c) provides an extended function to be minimized using the ensemble perturbation constraint as well as the static BEC. This approach is called the Hybrid Four-dimensional Ensemble-Variational data assimilation scheme (H4DEV). The ensemble control variable is operated, with Schur production, on ensemble trajectories consisting of the model variable, not the control variable. Just for the static BEC, the balanced temperature and surface pressure are derived through the nonlinear balance equation introduced in

Song et al. (2017b). First, the ensemble control variable is given vertical correlation, assigned by Gaspari and Cohn (1999)'s fifth-order correlation function with 0.2 log pressure, by a transform using the Eigen decomposition and the horizontal transform is applied to it. The localization length scale for H4DEV is approximately 3,600 km horizontally, which is wavenumber 10 in the spectral space. However, the localization scale in LETKF varies 660-1,800 km depending on the level. Song et al. (2017c) provided a more detailed description and their references address relevant principles. Figure 1 shows the flow chart of H4DEV analysis cycle. KPOP collects all possible observations, performs quality control and bias correction for satellite radiances using the high-resolution forecast at hourly intervals as the background, and provides corrected observations to both H4DEV and LETKF after horizontal, vertical, and temporal thinning. We use 50 ensemble samples in H4DEV to produce ensemble BEC, and the ensemble-to-static covariance ratio is 0.3:0.7 for hybrid BEC in H4DEV. Although the ensemble covariance ratio is set at 0.3, it gradually decreases above 20 km because the ensemble spread of the KIM ensemble forecasts is huge in the upper-level stratosphere and mesosphere. The large spread in the upper level seems to be characteristic of KIM. Changing the control variable from specific humidity to pseudo-relative
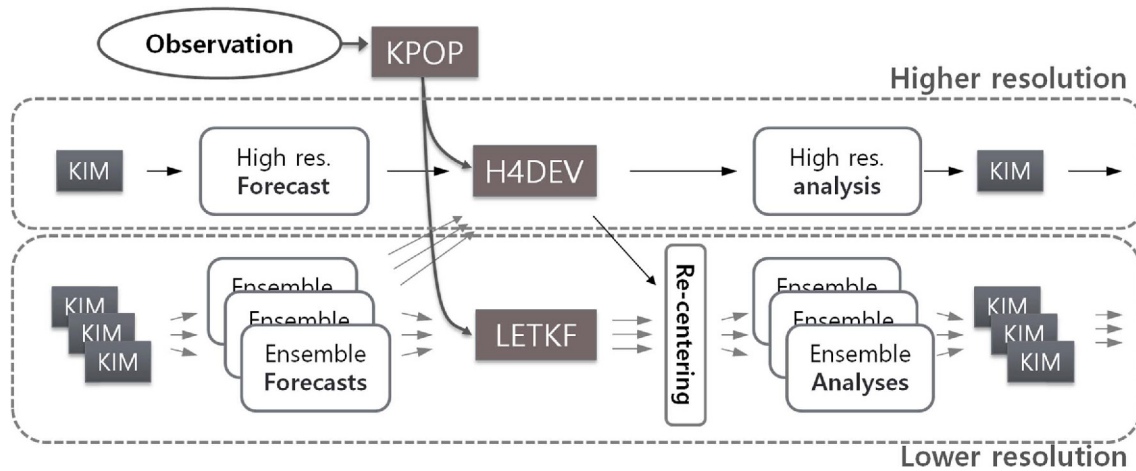
**Fig. 1.** Flow chart of the hybrid H4DEV analysis cycle system. The KPOP processes observations for both H4DEV and LETKF, and the recentering replaces the ensemble mean analysis with deterministic analysis. Presently, the high-resolution and low-resolution are respectively 12 km and 50 km horizontally, and the ensemble size is 50 members.

humidity in H4DEV is described in detail in Section 3c and, for technical description, Song et al. (2018; their Section 3c). After the LETKF process, the ensemble mean analysis is fully replaced by deterministic analysis in the recentering process. The current H4DEV version is coupled to a high-resolution deterministic model with resolution of 12 km, but the H4DEV analysis, ensemble model, and LETKF analysis resolutions were all 50 km. This paper discusses the operational configuration that accompanies the change to H4DEV (Table 1). The use of ensemble forecasts is the key difference between 3DVar and H4DEV.

3DVar is a global solver where conventional and non-conventional data are fitted simultaneously by increments relative to a background state. Since it uses a snapshot (three-dimensional) background, observation times within the analysis window is typically ignored. The relationship of model variables at different observation times (e.g., hourly) cannot be considered in the 3DVar framework. In contrast, the use of four-dimensional ensemble trajectories in H4DEV allows use of analysis increments closer to the observation times, and introduces temporal as well as spatial relationships between the analysis variables. The 3DVar framework was extended to utilize first-guesses at appropriate times (FGAT; Lee and Barker, 2005) within the analysis window, which is named 3DVar-FGAT. H4DEV shares the FGAT framework with 3DVar (3DVar-FGAT), so it can afford to analyze the hourly guesses.

The 3DVar minimization technique is a re-orthogonalized conjugate gradient method (Parlett, 1980). During minimization, H4DEV performs multiple outer loops with multiple resolutions. Four outer loops are executed with total wavenumber resolutions of 42, 85, 170, and 170, and its ensemble control variable participates in the minimization process after the second outer iteration (see Fig. 6 in Song et al., 2018), while 3DVar conducts a single outer loop with total wavenum-

ber 170. In other words, we conducted two 3DVar-FGAT minimizations—one each at T42 and T85—and then two H4DEV minimizations at T170. The full nonlinear model (or ensemble) is not re-run as a part of this process. This process, which only conducts re-linearization of the nonlinear observation operator, could be a shortage of being called outer loop, which strictly spoken additionally conducting re-integration of the nonlinear model; however, in this study, just the re-linearization of the observation operator is called outer loop for the convenience. Finally, the increment from the middle of the window is passed back to the model. The multiple outer loops method is beneficial for humidity variables with strong nonlinearity and small scale and provides a better guess and Jacobian. The guess can be updated closer to observations for each outer loop, and the Jacobian for radiances is computed using the updated guess to mitigate errors due to strong nonlinearities. The Jacobian in the 3DVAR is not updated in the minimization process because it is provided by KPOP, whereas H4DEV contains observation operators and hence can calculate a new Jacobian during minimization. The multiple resolution approach also has computational efficiency because it minimizes the cost function with low-resolution for the first and second outer loops. The accuracy is similar between full-resolution and multi-resolution outer-loop strategies because the early iteration in both tries to fit large-scale analysis increments to observations (Song et al., 2018). H4DEV added observation quality control in the process of minimization. The observations are evaluated with updated guess at the beginning of each outer loop, so the suspicious observations are removed and the eligible observations are restored, meaning that quality control decisions are redone as a part of the outer loop process. The number of observations differs for each H4DEV outer loop because the QC removes or restores observations.

Tropical cyclone (TC) initialization is also used in H4DEV. To make the analysis better represent the TC structure, Kleist
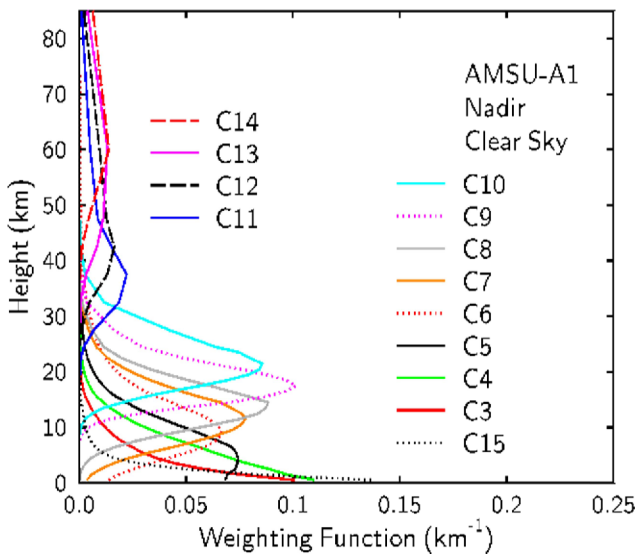
**Fig. 2.** The weighting function of AMSUA channels (http://profhorn. meteor.wisc.edu/wxwise/satmet/lesson12/hurrmicro1.html).

(2011) and Heming (2016) have assimilated TC advisory minimum sea level pressure. Based on these previous works, we assimilate a single value of minimum sea level pressure estimated from the Regional Specialized Meteorological Center (RSMC) Tokyo. Observation error varies linearly with TC intensity, where strong TC has larger observation error.

### d. Differences in the use of observations

Three ATMS water vapor channels are added in H4DEV-based system to improve the humidity performance, while 3DVar-based system assimilated only ATMS temperature channels. In the H4DEV-based system, high-latitude AMV from composite satellite observation is added. The AMVs derived from geostationary (GEO) satellite observations covers the middle latitudes and tropics, while AMVs over the polar region are derived from low-earth (polar) orbiting (LEO)

satellite. Thus, coverage between 60 and 70 degrees latitude is a gap in AMV observations. This was addressed by using AMVs derived from a combination of LEO and GEO satellite observations (LEOGEO AMV, Lazzara et al. 2014). Lee and Song (2018) have tested the LEOGEO AMV in the KIAPS DA system, and found the improvement of high-latitude wind performance. Therefore, The LEOGEO AMV observation has been added in H4DEV-based system to provide better spatial coverage for wind observation.

An important change in KIM that directly affects DA is that the model top was increased from about 60 to 80 km. Version 2.5 of the 3DVar-based system did not use upper channels 11-14 in Advanced Micro Sounding Unit-A (AMSU-A) because those observations degraded the performance. Those channels were affected by temperatures above 60 km depending on location (Fig. 2). If the model top was low, an observation operator cannot accurately calculate the brightness temperature of the upper channels from the background; hence the upper channels have been only sparsely considered previously. Since the model top was increased to 80 km in version 3.1, we assimilated those upper channels of AMSU-A and described the impact of these additional channels in Section 3d.

## 3. Evaluation of data assimilation changes

This section evaluates performance changes due to updating from 3DVar to H4DEV (Table 1). Two experiments—3DVar2.5+ and H4DEV3.1—were conducted using the same model (KIM version 3.1) in which the horizontal resolution was 25 km to see only the impact of DA changes (Table 2). The configuration of 3DVar2.5+ experiment is the same as version 2.5 of the 3DVar-based system, but 3DVar has hourly FGAT. Note that H4DEV experiment runs lower-resolution KIM compared to the version 3.1 system in Table 1. The experimental results have confirmed significant improvements in analysis fields from the update. Some additional experiments were conducted to see what specific updates improved performance.

**Table 2.** Description of experiments

| Experiment name | Description |
|---|---|
| H4DEV3.1 | The same as version 3.1 of the H4DEV-based system (See Table 1), but the resolution of KIM is 25 km |
| 3DVar2.5+ | The same as version 2.5 of the 3DVar-based system (See Table 1), but 3DVar has hourly FGAT and runs with the same KIM as H4DEV3.1 |
| 3DVar3.1 | The same as H4DEV3.1, but 3DVar-FGAT with a single outer-loop |
| H4DEV3.0 | H4DEV version 3.0 which does not include multiple outer-loops, pseudo-RH, new observations, Innovation QC, TC initialization, and partial recentering |
| LETKF3.0 | LETKF version 3.0 |
| RECNT_P | Partial recentering applied to H4DEV3.0 |
| RECNT_F | Full recentering applied to H4DEV3.1 |
| H4DEV3.0b | H4DEV version 3.0b which includes pseudo-RH, new observations except AMSU-A channels 11 - 14, Innovation QC, TC initialization, and partial recentering |
| H4DEV3.0b_NPRH | H4DEV version 3.0b which does not include pseudo-RH |

## (a) Zonal wind



## (b) Meridional wind
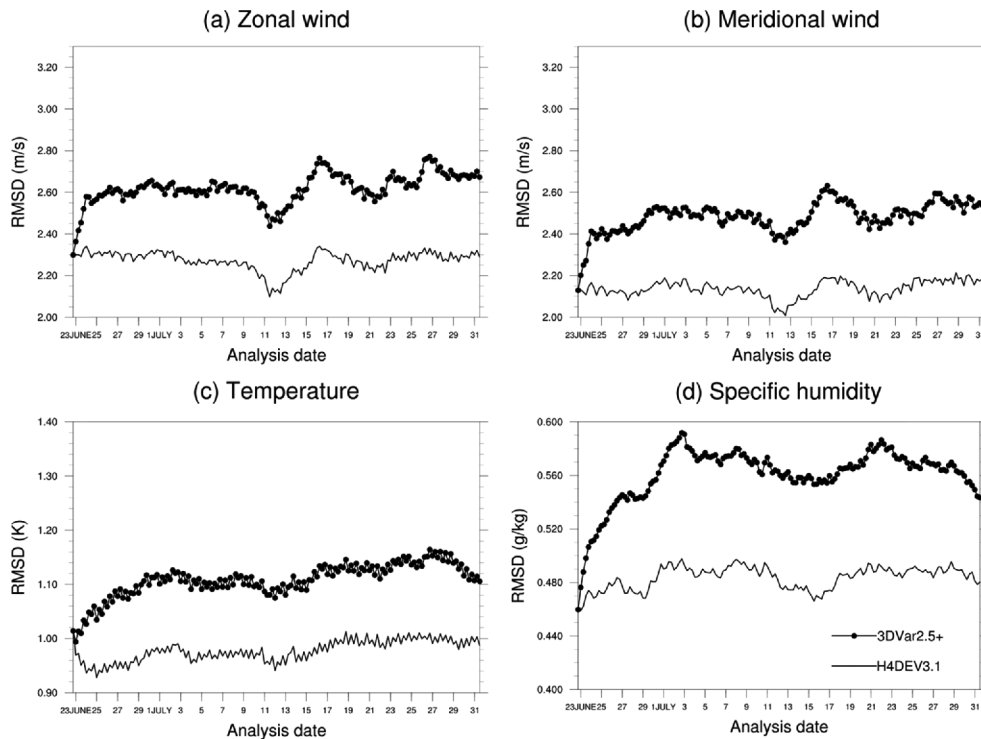


## (c) Temperature



## (d) Specific humidity



**Fig. 3.** The time series of the root-mean-squared difference (RMSD) comparison between 3DVar2.5+ and H4DEV3.1 analyses for zonal (a) and meridional (b) winds (m s$^{-1}$), temperature (c; K), and specific humidity (d; g kg$^{-1}$). The RMSD is calculated against the IFS analysis for 1000-10 hPa. The differences between the two experiments are as shown in Table 2. The analysis-forecast cycle started at 1800 UTC on 22 June 2017.

### a. Assessment of full data assimilation system update

Both 3DVar2.5+ and H4DEV3.1 experiments were conducted from 1800 UTC 22 June to 1200 UTC 31 July 2017. The initial background for the first cycle was six-hour forecasts using KIM with the initial condition from the Unified Model (UM) analysis from KMA valid at 1200 UTC 22 June 2017. Figure 3 shows the time series of the root mean squared difference (RMSD) of analysis for both experiments. The RMSD was calculated against the analysis of the ECMWF integrated forecasting system (IFS) and averaged up to 10 hPa. The improvement caused by the DA system update was significant for all variables throughout the entire period. The DA update reduced the zonal and meridional winds, temperature and mixing ratio errors by 10.1%, 12.8%, 13.9%, and 13.7%, respectively. Although the 3DVar2.5+ RMSD increased rapidly for several days, H4DEV3.1 RMSD remained similar to the initial state until the end.

Figure 4 shows zonal means of the differences in RMSD between H4DEV3.1 and 3DVar2.5+ for each variable. The DA update contributes to reducing the analysis error for wind in the upper troposphere, moisture and temperature in the tropical mid-troposphere. The accurate boundary-layer humidity enables the more accurate diagnosis of convective motion linking lower-level improvement with free atmosphere wind accuracy.

The additional inclusion of upper-level AMUS-A channels (11-14) adjusts the mid-/upper- stratospheric temperature and horizontal winds. The difference between 3DVar- and H4DEV-based systems can be attributed partially to each update in the series of developments.

Figure 5 verifies the performance against observations. The bias was calculated as the background minus observation and averaged over the entire period. Wind speed performance was evaluated by aircraft (Fig. 5a) and Sonde (Fig. 5d). The smaller standard deviation of H4DEV3.1 for both observations corresponds to the smaller wind speed RMSD in Fig. 4a. We can also see that the model has little wind speed bias in the upper levels but positive wind speed bias in the lower levels. In addition to the Sonde temperature observation (Fig. 5e), the AMSU-A brightness temperature (Fig. 5b) and GPS-RO bending angle (Fig. 5c) are useful for evaluating the model temperature accuracy. The background of H4DEV3.1 is relatively close to the observation because the standard deviation is smaller for all three observations. In particular, the standard deviation for the AMSU-A upper channels has been greatly reduced because H4DEV3.1 assimilates channels 11-14. Although the standard deviations of temperature are smaller at all levels, AMSU-A channels 10-11 have negative TB bias. Figure 5e shows that the background temperature of H4DEV3.1 has a negative bias as the altitude increases to 50 hPa. It confirms that
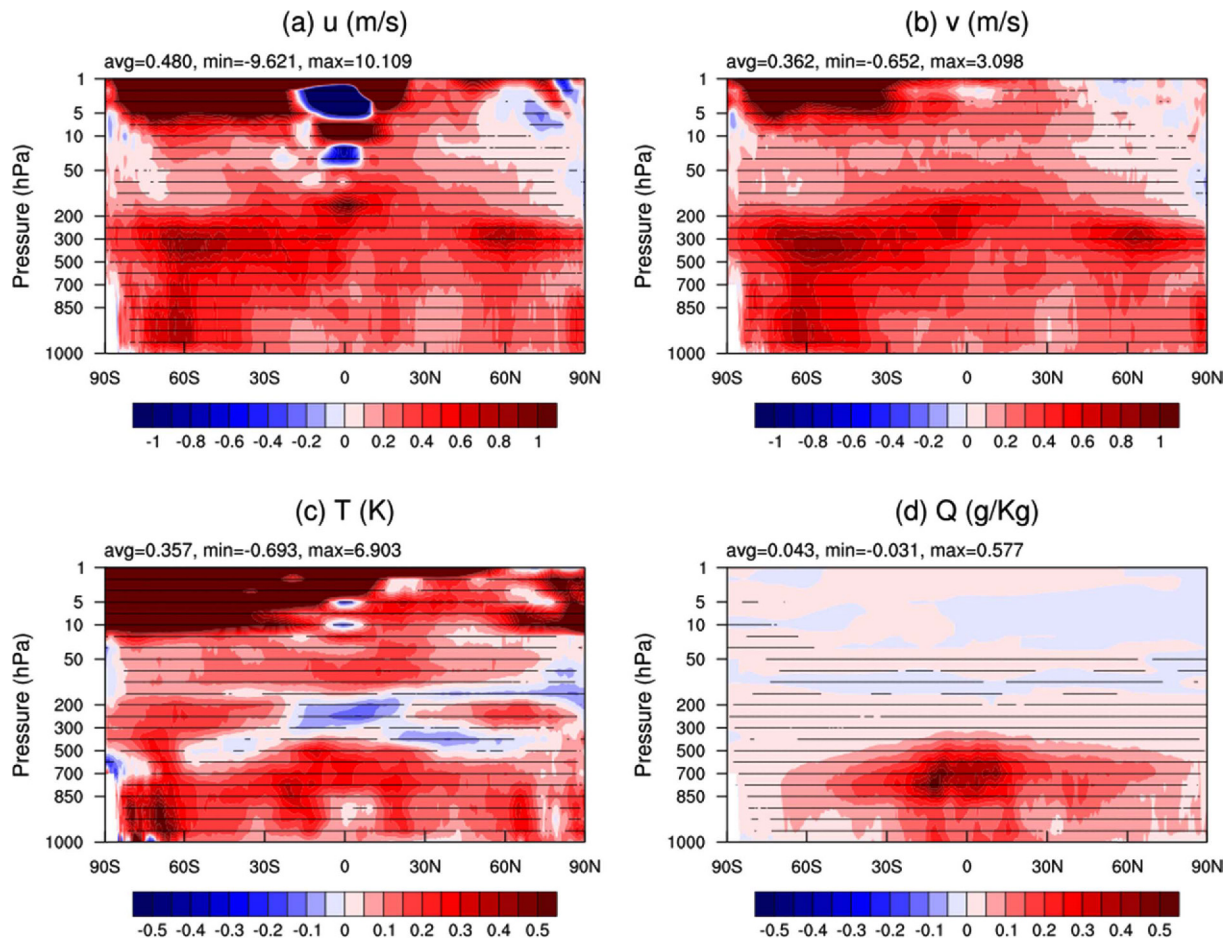
**Fig. 4.** Cross-section of the RMSD reduction of H4DEV3.1 analysis compared to the 3DVar2.5+ analysis for zonal (a) and meridional (b) winds (m s$^{-1}$), temperature (c; K), and specific humidity (d; g kg$^{-1}$), which is a composite of 156 fields since 1800 UTC 22 June 2017. Red color (positive values) indicates the variables and regions for which H4DEV3.1 surpasses the analysis skill of 3DVar2.5+.

the humidity of H4DEV3.1 is closer to observations (Fig. 5f).

As shown in Fig. 4c, temperature performance is improved in most areas but degrades at around 250 hPa in the tropics. We identified the cause of this increased RMSD by comparing 3DVar2.5+ and H4DEV3.1 biases (Figs. 6a, c). As expected from the negative bias in the observation verification with the Sonde temperature, the analysis of H4DEV3.1 has a negative temperature bias in this region. It can be assumed that the new DA makes the area cooler because both experiments use the same model. However, we found that H4DEV3.1 significantly increases the temperature around 250 hPa during the DA process (Fig. 6d) compared to 3DVar2.5+ (Fig. 6b). It should be noted that the temperature bias is at a low level around the tropics. 3DVar has a positive bias in low levels, whereas H4DEV3.1 has very little bias. Normally, warm temperature in low levels accelerates convection above the area, which can increase the temperature in the upper levels. In contrast, a colder temperature in low levels for H4DEV3.1 causes less convection and the upper-level temperature is hence cooler than for 3DVar2.5+. Relatively small amount of convective

rain proves that the convection is reduced around the tropics (Fig. 7). Consequently, H4DEV3.1 reduces the bias at both the low and middle levels with appropriate analysis increments during the DA process, but the model increases the negative temperature bias at the middle levels.

Figure 8 shows the impact of the DA update on the forecast skill as measured by the geopotential height anomaly correlation. More accurate analysis improved the forecast over five days for all regions except the tropics. The anomaly correlation at 500 hPa on day five was 0.76 for 3DVar2.5+, but 0.81 for H4DEV3.1 in the northern hemisphere. Note that this is different from the operational performance due to the lower KIM horizontal resolution.

### b. Impact of the data assimilation replacement

Figure 9 shows the results from H4DEV3.1 and the 3DVar3.1, which is the same as the H4DEV3.1 but uses the 3DVar-FGAT technique (see Table 2). The H4DEV3.1 improves the analysis for all model variables in most regions aside from the South
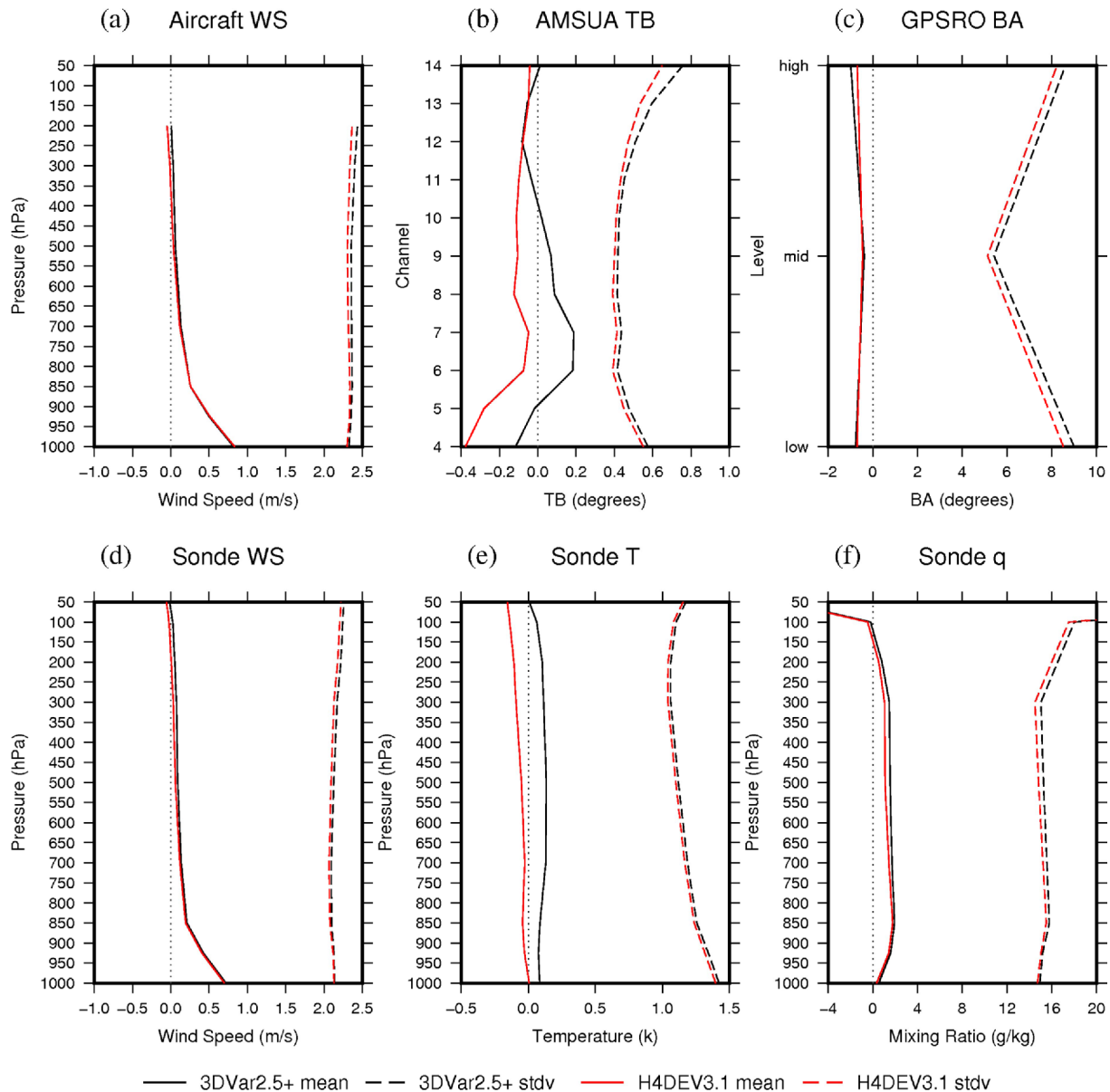
**Fig. 5.** The bias (solid curves) and standard deviation (dashed curves) of background (six-hour forecast) error with respect to the wind speed observations from aircraft (a) and Sonde (d), brightness temperature (b) from AMSU-A, the bending angle (c) from GPS-RO, and the temperature (e) and mixing ratio (f) from Sonde. Red and black colors denote H4DEV3.1 and 3DVar2.5+, respectively. The low, mid, and high in the y-axis of the GPS-RO figure denote below 10 km, 10-40 km, and above 40 km, respectively.

Pole and 250 hPa over the tropics for temperature (Fig. 9c) and the lower-stratospheric zonal wind (Fig. 9a). The broad improvement in horizontal winds and temperature in the southern hemisphere is consistent with Song et al. (2017c, Figs. 2, 3); one deviation compared to their study is a significant improvement in the arctic upper troposphere winds (Figs. 9a, b).

As discussed in Song et al. (2017c), the two-way coupling strategy (in which the LETKF analysis ensemble is recentered around the H4DEV analysis rather than another deterministic analysis such as 3DVar) for the BEC hybridization can enhance the H4DEV performance relative to the 3DVar-FGAT. The realized example is said to be the arctic upper-tropospheric wind and temperature advantages as mentioned before.

### c. Strategies related to humidity improvement

The first released H4DEV version (H4DEV3.0) did not implement all changes in Table 1, and although wind and temperature performance were significantly improved, humidity performance was hardly improved. Therefore, we compared
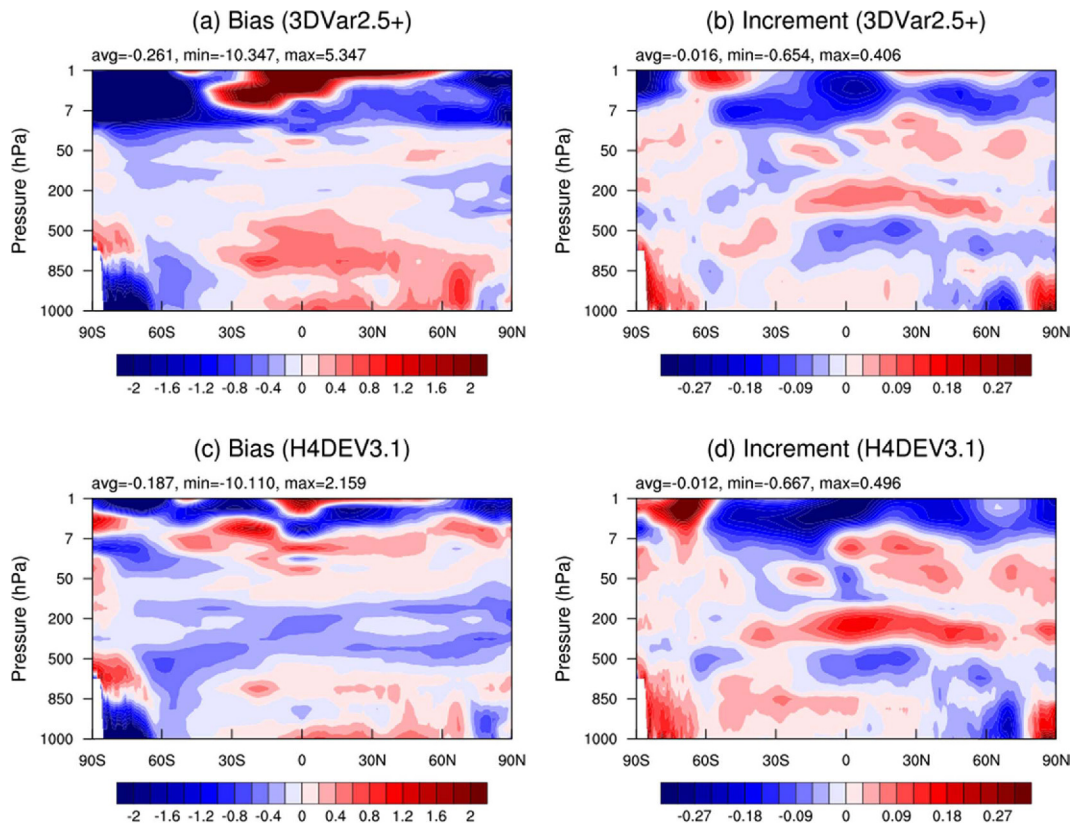
**Fig. 6.** Cross-section of the analysis bias against IFS analysis of 3DVAR2.5 (a) and H4DEV3.1 (c), and the analysis increments of 3DVar2.5+ (b) and H4DEV3.1 (d) for temperature.
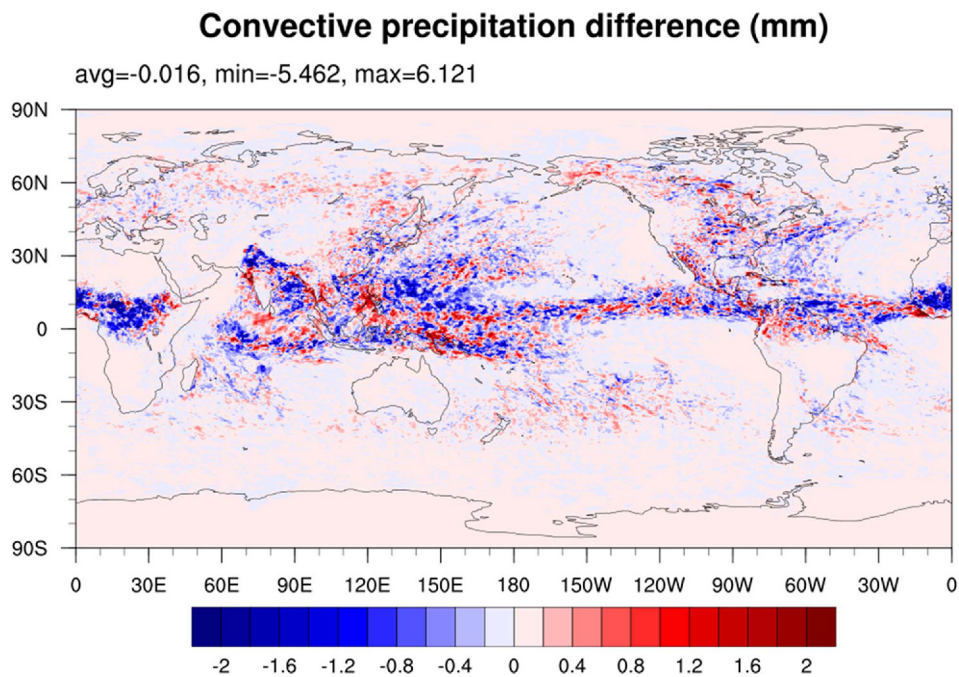


**Fig. 7.** Convective precipitation difference which is a composite of 6-hour accumulated convective rain (mm) from initials of July 2017. The average of the difference is negative 0.015 mm. Blue color (negative values) indicates that the less convective rain in H4DEV3.1 than 3DVar2.5+.
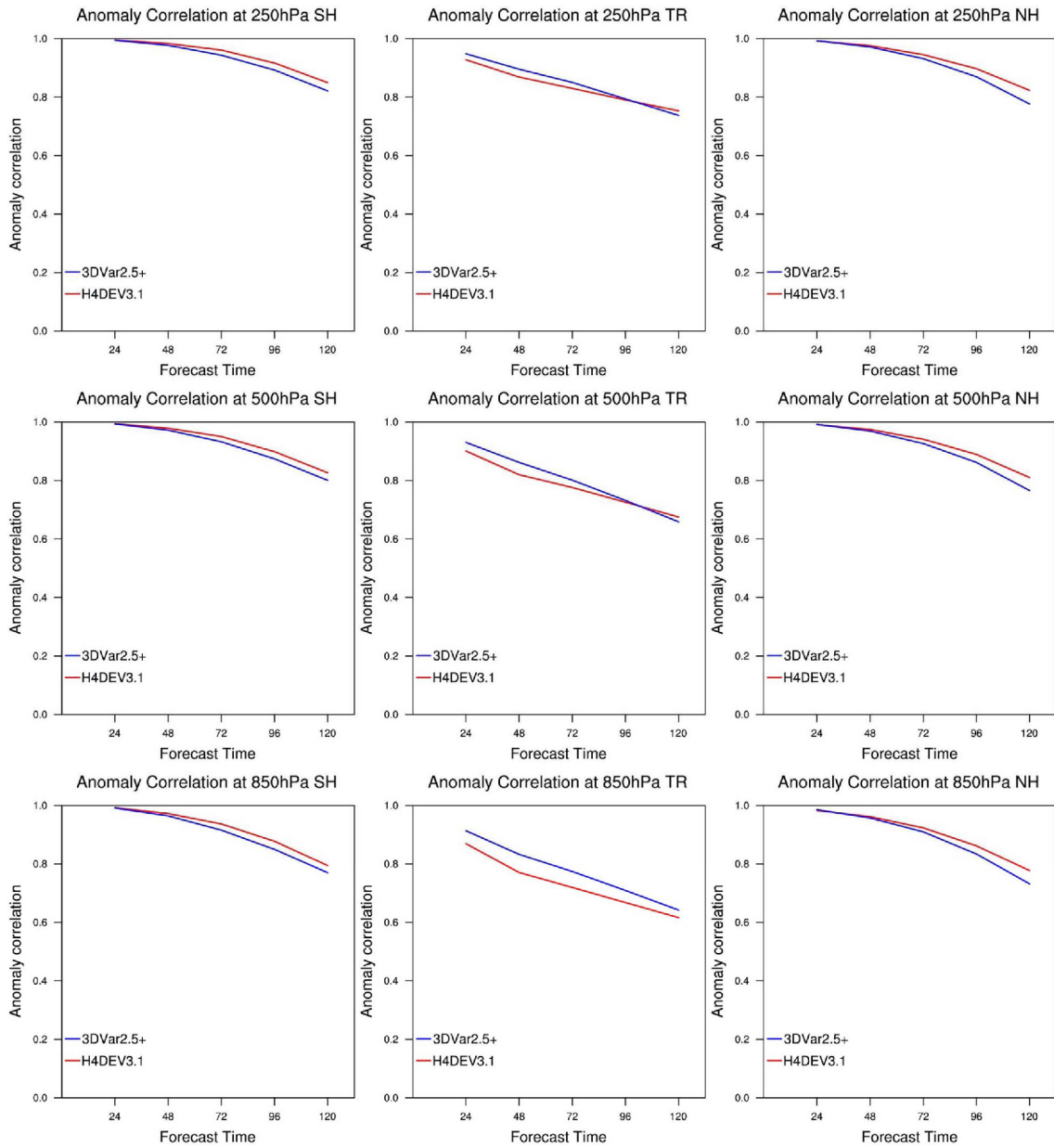
**Fig. 8.** Anomaly correlation for the geopotential height of 3DVar2.5+ (red line) and H4DEV3.1 (blue line) through five-day forecast.

H4DEV3.0 and LETKF3.0 to identify ways of improving the humidity performance. Figure 10 compares H4DEV3.0 and LETKF3.0 accuracy for 21-28, March 2017. Although H4-DEV3.0 and LETKF3.0 have similar wind performance, LETKF3.0 has clearly better humidity performance. The solid lines are the RMSD of the ensemble mean of 50 LETKF analyses while the dashed lines are the H4DEV3.0 analysis. A fair comparison was ensured by calculating the average of each RMSD for 50 LETKF analyses (gray lines). Normally, the average of each RMSD is greater than the RMSD of the average of the errors. Nevertheless, the H4DEV3.0 humidity error is still greater than the average of the LETKF3.0 humidity

error. The improved humidity performance of LETKF3.0 is because the BEC of the humidity can be better estimated with ensemble forecast samples. Furthermore, LETKF has a smaller localization length scale, which is useful for variables with strong heterogeneity such as the humidity.

(1) Impact of partial humidity recentering

In situations where LETKF has better humidity performance than H4DEV, we have considered a partial recentering to take advantage of the LETKF technique for humidity. Instead of completely replacing the whole ensemble mean with deterministic analysis, we have tried a 50% replacement just for
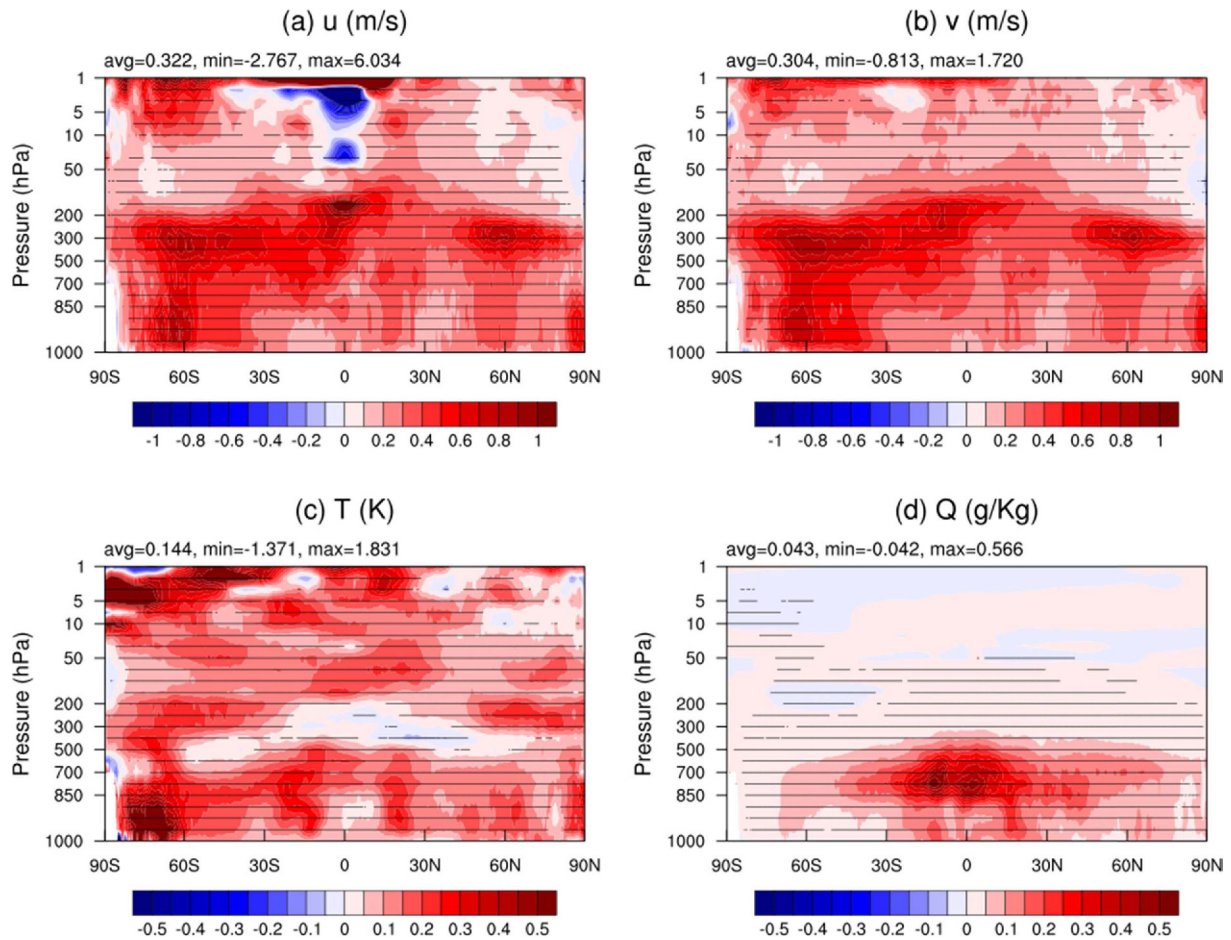
**Fig. 9.** The same as Fig. 4 except the RMSD is reduced by changing only the DA technique (From 3DVar with a single outer-loop to H4DEV with multiple outer-loops).

humidity. Thus, the humidity average of the initial conditions for the ensemble models is the mean of the ensemble mean analysis and deterministic analysis, unlike other variables. Bowler et al. (2017) confirmed that fully recentering ensemble samples around the high-resolution analysis is an important benefit in their ensemble 4DEnVar. However, this recentered system showed slightly lower forecast skill than their ensemble transform Kalman filter (ETKF) due to the fact that the spread of the ensemble samples is less than the spread of the ETKF ensemble. The ensemble BEC can better analyze humidity because the humidity variable is highly flow-dependent and its scale is relatively small. Although the H4DEV uses the ensemble BEC, its ratio is only 0.3 and the localization length scale is larger than LETKF. We did the same experiment with H4DEV for the same period but applied partial recentering for humidity. Figure 11 shows the partial recentering performance; not only is the accuracy of the humidity greater than in the experiment with full recentering, but the wind and temperature performance were similar or better in the partial recentering experiment. The partial recentering has a direct impact on the ensemble forecasts, and the improved ensemble can affect the

hybrid BEC in the next DA cycle. The partial recentering of humidity may cause some imbalance between the humidity and the wind or temperature in the model initial condition. However, it is reasonable to deduce that the balance is restored during the model evolution. Furthermore, partially recentered humidity is better balanced with cloud water contents because there is no change in the cloud water contents and the humidity increment is relatively small.

(2) Impact of the implementation of pseudo-relative humidity (RH)

Pseudo-RH has been adopted to increase the representativeness of the interpolation process for humidity observation and to improve the Gaussianity of the moisture background error characteristics (Dee and Da Silva 2003; Song et al., 2018). In contrast with the specific humidity, the relative humidity broadens the effective radius of the moisture error correlation; relatively, the interpolation error that originates from fitting to conventional (Sonde and Surface data) moisture observations (its distribution can be found in Fig. 4 of Kang et al. (2018)) is reduced. The moisture quality improvements in
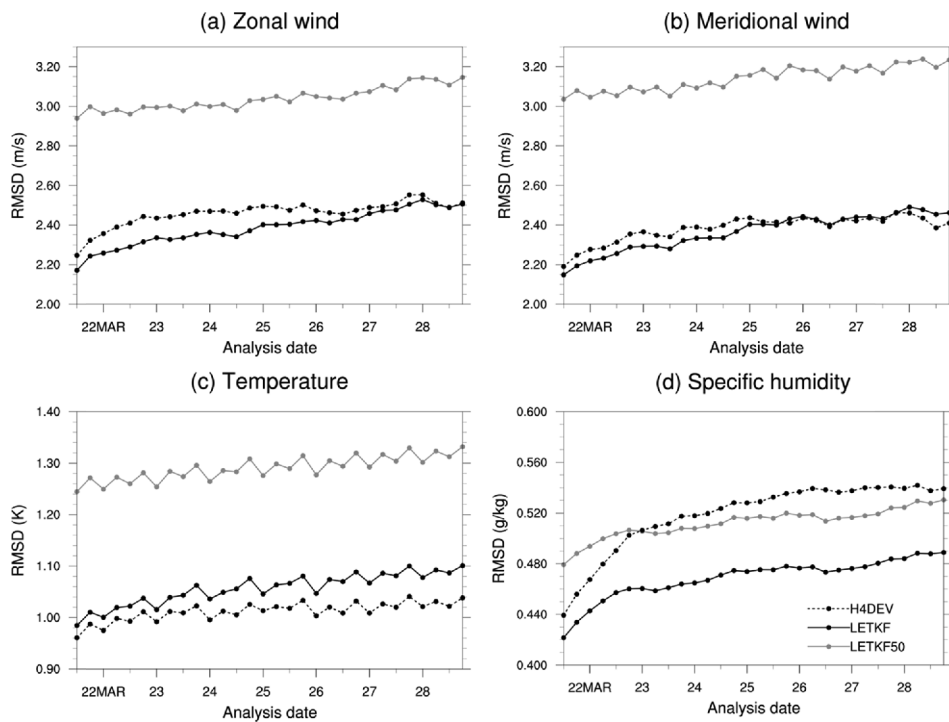
**Fig. 10.** The time series of the RMSD comparison between H4DEV and LETKF alone cycles. The dotted line represents the early version of H4DEV (experiment H4DEV3.0), and the black and gray solid lines are the RMSD of the ensemble mean and the average of 50 ensembles' RMSD generated by LETKF (experiment LETKF3.0), respectively. The analysis-forecast cycling started at 1200 UTC on 22 March 2017.
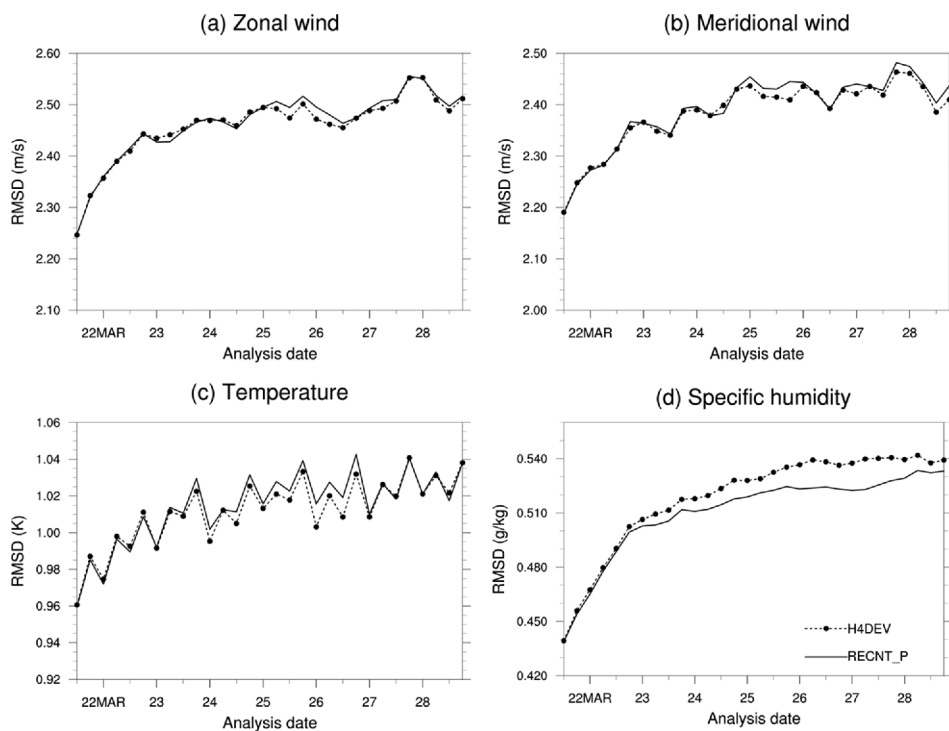


**Fig. 11.** The same as Fig. 9 except for the comparison between full recentering (dotted line) and partial recentering (solid line) in experiment H4DEV3.0.
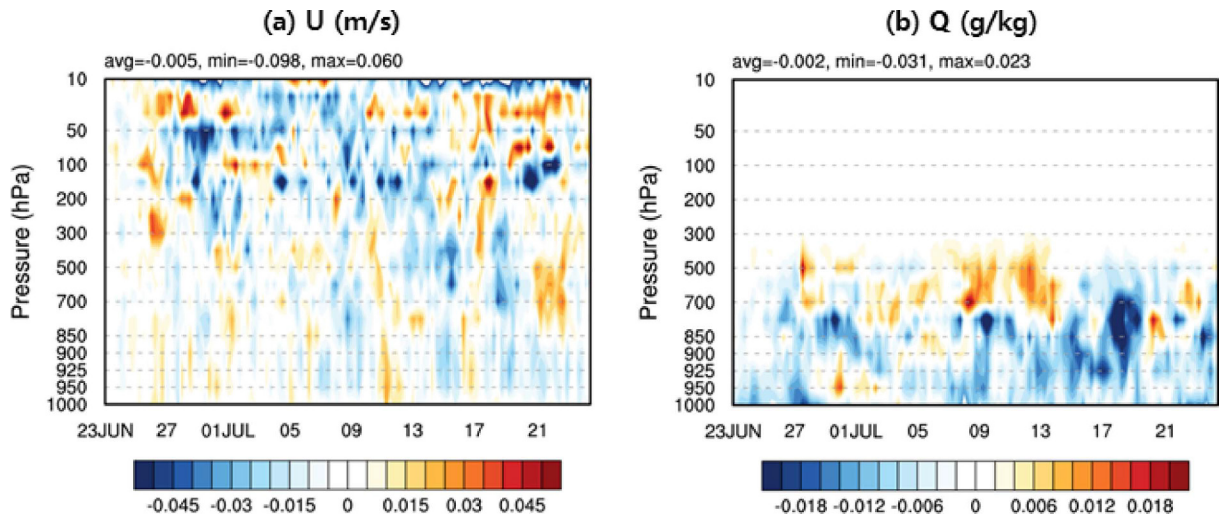
## (a) U (m/s)

avg=-0.005, min=-0.098, max=0.060

## (b) Q (g/kg)

avg=-0.002, min=-0.031, max=0.023



**Fig. 12.** Difference in the background RMSD calculated over latitude-longitude axes as a function of the time and level between the cases in which the specific humidity (H4DEV3.0b_NPRH) or pseudo-RH (H4DEV3.0b) was used for the humidity control variable. The blue color represents that the adoption of pseudo-RH shows positive impacts in zonal wind (a; m s$^{-1}$) and specific humidity (b; g kg$^{-1}$). The analysis cycle configuration is the same as in Fig. 8 except for the moisture control variable.

### (a) Zonal wind

### (b) Meridional wind

### (c) Temperature

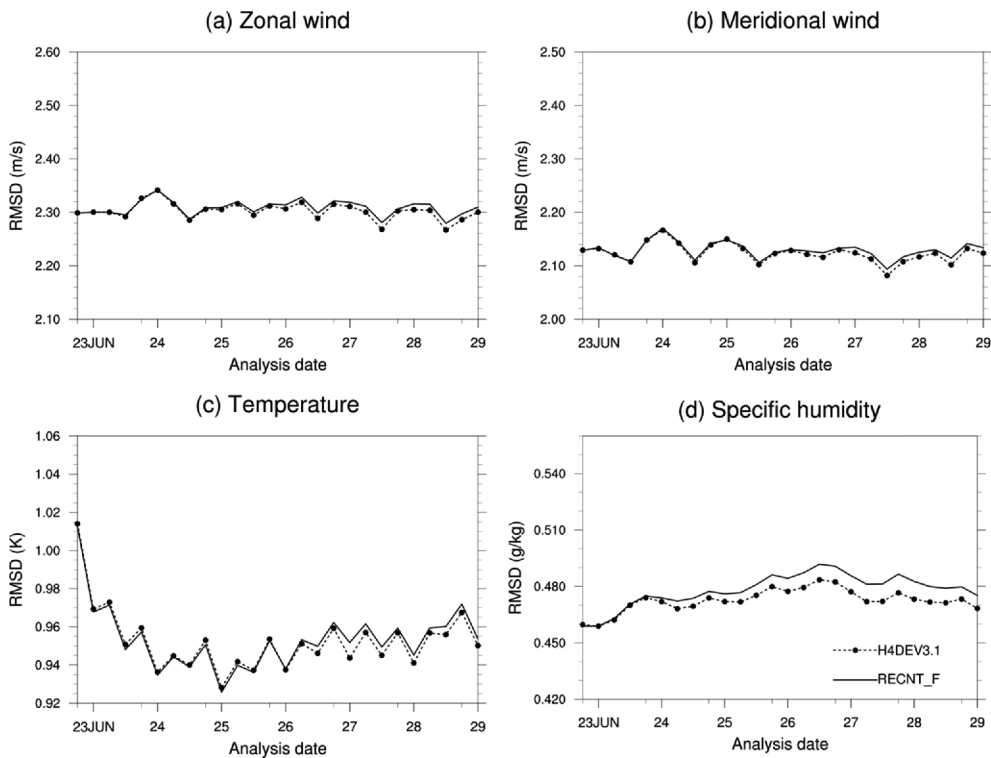### (d) Specific humidity



**Fig. 13.** The same as in Fig. 3 except it is a comparison between partial recentering (dotted line) and full recentering (solid line) in the experiment H4DEV3.1.

the boundary-layer shown in Fig. 12 come partly from the accurate calculation of the observation innovation for humidity. The negative feature in the mid-/upper-moisture ends up having a neutral impact on the cycling analysis. For reference, this experimental result comes from the comparison between

H4DEV3.0b_NPRH and H4DEV3.0b as shown in Table 2.

Deviation from Gaussianity is necessarily related to the appearance of skewness in the probability distribution of the moisture background. With considering the analysis increment solely obtained from the information of the mean and the

covariance (the first and second moments of the probability distribution), the asymmetric correction depending on the skewness can be allowed by incorporating non-Gaussianity into the variational framework (Fletcher, 2010) or a serial ensemble Kalman filter (Bishop, 2016) or by implementing a particle filter. Pseudo-RH has a more similar shape to the Gaussian distribution in contrast to the specific humidity. Thus, there can be a distinct improvement in dry and cloudless regions where the near-zero values on a tail create an unbalanced heavy weighting in the probability. In addition to this kind of physical variable transform approach for preserving Gaussianity, there is analytic function-based transform approach such as Gaussian anamorphosis (Amezcua and Van Leeuwen, 2014).

We would expect improvements in the H4DEV humidity analysis caused by adopting pseudo-RH to reduce the impact of partial recentering. The impact of the partial recentering after changing to pseudo-RH is as illustrated in Fig. 13. As shown there, partial recentering still apparently works for decreasing the humidity analysis RMSD; this implies that the recentering strategy has room for analysis improvement, even in the configuration of a new humidity control variable.

### d. Impact of assimilation of middle atmospheric microwave observation

In March 2018, the top model level of KIM was raised from 60 km to 80 km (Hong et al., 2018). As shown in Fig. 2, the microwave sounding from AMSU-A has non-negligible weighting above 60 km. Thus, the usability of the upper channels (11-14) was expected to improve the mid-/upper-stratospheric forecast skill. However, KIM offers a poor-quality background at observation-sparse levels (above 60 km), which makes it difficult to apply an effective air-mass-based bias correction. Therefore, it is decided that only scan bias correction is carried out for channels 11-13, unlike in the other operational center. There is no bias correction for channel 14 in our strategy, which is the same as most other operational centers.

Extending the useful range of numerical model forecasts beyond around 10 days and into the sub-seasonal time-scale is a major research issue for modern numerical weather prediction. The strong stratospheric polar vortex results in autocorrelations at sub-seasonal time-scales and the tropospheric jet is affected by anomalous changes in the stratospheric vortex within this time-scale (Tripathi et al., 2014). In addition, Arctic Oscillation response to the stratospheric Quasi-Biennial Oscillation can modulate the atmospheric prediction on seasonal-to-multiannual timescales (Marshall and Scaife, 2009). Therefore, middle atmospheric dynamics is a key link between short-range and extended-range weather forecasts and between the actively mixed layer and departed density layers in the atmosphere (Tripathi et al., 2014). The impact of the variation in the polar vortex alters the strength and phase of jet streams so that the short-range baroclinic waves that disturb weather systems vary in turn.

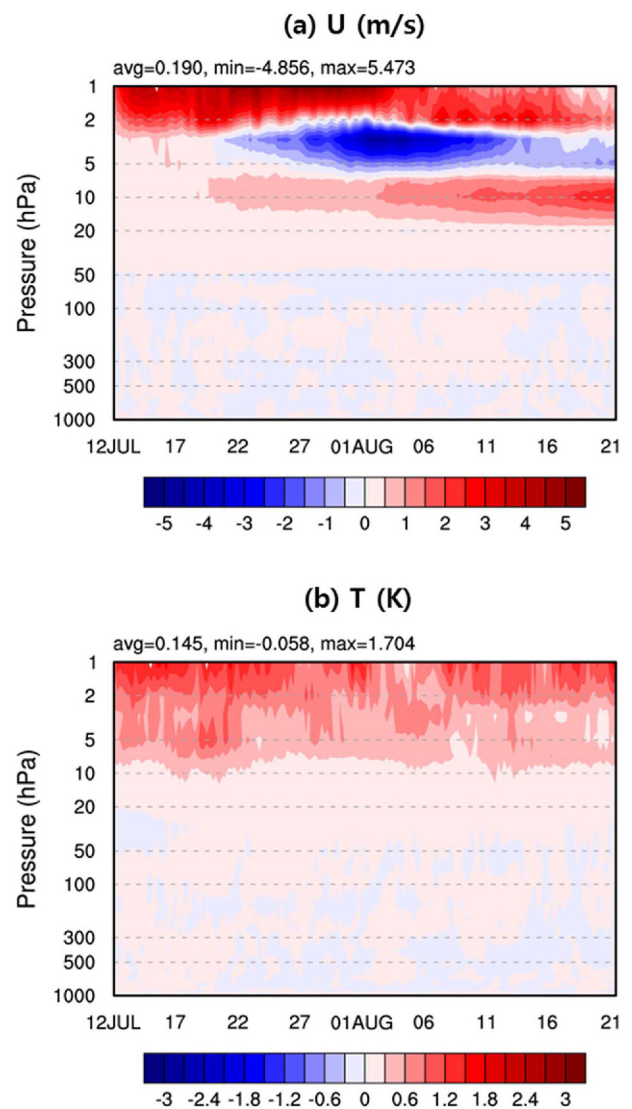The impact of the middle atmosphere correlations accu-



**Fig. 14.** The same as Fig. 11 except for the objective to be evaluated, DA schemes used, and experiment period. Here, the red color shows where the upper-level AMSU-A channels (11-14) reduce the analysis RMSD of zonal wind (a; m s$^{-1}$) and temperature (b; K) against IFS analysis relative to the denial experiment. For both experiments (the addition of upper-level channels versus denial), 3DVar-FGAT was used for the DA scheme. The analysis-forecast cycling started at 0000 UTC on 12 July 2017.

mulates through continuous analysis-forecast cycling (Fig. 14). As well as the temperature itself, for which the AMSU-A upper-channel observation provides information mainly, zonal wind centered around 10 hPa has been improved as the analysis-forecast cycle repeats (Fig. 14a). The indirectly induced mid-stratospheric zonal wind information from the BEC structure and consecutive six-hour forecasts (Polavarapu and Pulido, 2015) consistently contribute to reducing the background error in the repeated cycling of the incorporation of upper-level AMSU-A channels.

However, the significant degradation around 2-5 hPa is also

found. The relationship between temperature and horizontal wind is partly determined by horizontally geostrophic and vertically hydrostatic balances (thermal wind balance; Holton 2004). The 3DVar-FGAT with regressed balance equation (Wu et al., 2002; Song et al., 2017b) and hydrostatic relationship (Derber and Bouttier, 1999) considers the thermal wind balance in an expanded way, even including nonlinear advection. However, the thermal wind relationship applies only weakly in the tropics, particularly in the upper level (refer to Fig. 2 in Song et al., 2017b); the negative impact appears around 5 hPa in the experiment about the stratospheric channels of AMSU-A. Potentially, use of ensemble information (currently, the sensitivity test of upper-level AMSU-A channels is conducted in the 3DVar-FGAT frame.) could contributes to reducing this negative impact of the wind information extraction from the satellite-derived temperature. This issue will be investigated in the near future.

## 4. Conclusions and discussion

This study demonstrates the development history of the KIAPS operational DA system through its successful and consistent skill improvements. The improvement arising from the full DA update was significant for the zonal and meridional winds, temperature and mixing ratio throughout the entire period. The DA scheme change from 3DVar to H4DEV brings out overall enhancements in the operational DA performance. Since Figs. 4 and 8 have similar patterns and amplitude, it can be seen that impact of the scheme change accounts for most of the performance improvement. The biggest difference between Figs. 4 and 8 is wind and temperature above 10 hPa. This was caused by assimilation of AMSU-A channels 11-14. The upper-level AMSU-A channels correct the temperature and horizontal winds indirectly through background error specification so that stratospheric phenomena can be better simulated to demonstrate the intrusion of the positive signal into the lower-atmospheric level. Another difference two figures is error reduction of zonal wind around Jetstream regions. High-latitudinal (60-70°) wind analysis improvements can be attributed to LEOGEO AMVs.

The coupling strategy for the hybridization of the humidity analysis between H4DEV and LETKF and the adoption of the pseudo-RH improve the quality of the H4DEV moisture analysis. Furthermore, we have tested the partial recentering experiment with a single recentering weight as 0.5 for only humidity. Although the improvements have been made to the humidity analysis in this study, a more sophisticated study of partial recentering is required in part to find reason and optimize performance.

After raising the model top from 60 to 80 km, AMSU-A channel 11-14 were assimilated, giving improved temperature forecasts above 10 hPa. Following assimilation of the upper AMSU-A upper channels, the ATMS upper channels will be assimilated soon. Since ATMS channels 12-15 are similar to the AMSU-A channel 11-14, some additional improvement is

expected.

Future plans for KIAPS DA are four-dimensional incremental analysis updates (4DIAU), variational bias correction (VarBC), and increasing the ensemble size and resolution. The 4DIAU is expected to mitigate the spin-up caused by the imbalance of initial conditions in the early stages of model evolution. The VarBC is currently under development and has been applied to AMSU-A, which significantly reduces the differences between observation and analysis. This will be operational after further evaluation for both summer and winter seasons. H4DEV will employ a time-lagged ensemble method using the members of the previous prediction that are valid for the analysis time to get a larger ensemble size at a lower cost. After increasing the ensemble size and resolution, we will try to increase the ratio of ensemble BEC in H4DEV. We are planning to apply variable localization length-scales on each outer-loop according to its spectral resolution, of which results will be appeared in the future.

**Edited by:** Song-You Hong

## References

Amezcua, J., and P. J. Van Leeuwen, 2014: Gaussian anamorphosis in the analysis step of the EnKF: a joint state-variable/observation approach. *Tellus A*, **66**, 23493, doi:10.3402/tellusa.v66.23493.

Bishop, C. H., 2016: The GIGG-EnKF: ensemble Kalman filtering for highly skewed non-negative uncertainty distributions. *Quart. J. Roy. Meteor. Soc.*, **142**, 1395-1412, doi:10.1002/qj.2742.Bonavita, M., E. Hólm, L. Isaksen, and M. Fisher, 2016: The evolution of the ECMWF hybrid data assimilation system. *Quart. J. Roy. Meteor. Soc.*, **142**, 287-303, doi:10.1002/qj.2652.

Bormann, N., A. Geer, and T. Wilhelmsson, 2011: Operational implementation of RTTOV-10 in the IFS. ECMWF Tech. Memo. 650, Reading, UK, ECMWF, 23 pp.

Bowler, N. E., and Coauthors, 2017: Inflation and localization tests in the development of an ensemble of 4D-ensemble variational assimilations. *Quart. J. Roy. Meteor. Soc.*, **143**, 1280-1302, doi:10.1002/qj.3004.

Buehner, M., 2005: Ensemble-derived stationary and flow-dependent background-error covariances: Evaluation in a quasi-operational NWP setting. *Quart. J. Roy. Meteor. Soc.*, **131**,1013-1043.

Buehner, M., J. Morneau, and C. Charette, 2013: Four-dimensional ensemble-variational data assimilation for global deterministic weather prediction. *Nonlin. Processes Geophys.*, **20**, 669-682, doi:10.5194/npg-20-669-2013.

_____, and Coauthors, 2015: Implementation of deterministic weather forecasting systems based on ensemble-variational data assimilation at Environment Canada. Part I: The global system. *Mon. Wea. Rev.*, **143**, 2532-2559, doi:10.1175/MWR-D-14-00354.1.

Choi, S.-J., F. X. Giraldo, J. Kim, and S. Shin, 2014: Verification of a non-hydrostatic dynamical core using the horizontal spectral element

method and vertical finite difference method. *Geosci. Model Dev.*, **7**, 2717-2731, doi:10.5194/gmd-7-2717-2014.

Clayton, A. M., A. C. Lorenc, and D. M. Barker, 2013: Operational implementation of a hybrid ensemble/4D-Var global data assimilation system at the Met Office. *Quart. J. Roy. Meteor. Soc.*, **139**, 1445-1461, doi:10.1002/qj.2054.

Culverwell, I. D., H. W. Lewis, D. Offiler, C. Marquardt, and C. P. Burrows, 2015: The Radio Occultation Processing Package, ROPP. *Atmos. Meas. Tech.*, **8**, 1887-1899.

Dee, D. P. and A. M. Da Silva, 2003: The choice of variable for atmospheric moisture analysis. *Mon. Wea. Rev.*, **131**, 155-171.

Derber, J., and F. Bouttier, 1999: A reformulation of the background error covariance in the ECMWF global data assimilation system. *Tellus A*, **51**, 195-221, doi:10.3402/tellusa.v51i2.12316.

Fletcher, S. J., 2010: Mixed Gaussian-lognormal four-dimensional data assimilation. *Tellus*, **62**, 266-287, doi:10.1111/j.1600-0870.2009.00439.x.

Gaspari, G., and S. E. Cohn, 1999: Construction of correlation functions in two and three dimensions. *Quart. J. Roy. Meteor. Soc.*, **125**, 723-757. doi:10.1002/qj.49712555417.

Heming, J. T., 2016: Met Office Unified Model tropical cyclone performance following major changes to the initialization scheme and model upgrade. *Wea. Forecasting*, **31**, 1433-1449, doi:10.1175/WAF-D-16-0040.1.

Hocking, J., P. Rayer, R. Saunders, M. Matricardi, A. Geer, and P. Brunel, 2012: RTTOV v10 Users Guide. NWPSAF-MO-UD-023, 92 pp.

Holton, J. R., 2004: *An Introduction to Dynamic Meteorology.* Elsevier, 535 pp.

Hong, S.-Y., and Coauthors, 2018: The Korean Integrated Model (KIM) system for global weather forecasting (in press). *Asia-Pac. J. Atmos. Sci.*, **54**, doi:10.1007/s13143-018-0028-9.

Hunt, B., E. Kostelich, and I. Szunyogh, 2007: Efficient data assimilation for spatiotemporal chaos: A local ensemble transform Kalman filter. *Physica D*, **230**, 112-126, doi:10.1016/j.physd.2006.11.008.

Kang, J.-H., H.-W. Chun, S. Lee, H.-J. Song, J.-H. Ha, I.-H. Kwon, H.-J. Han, H. Jeong, and H.-N. Kwon, 2018: Development of an observation processing package for data assimilation in KIAPS (in press). *Asia-Pac. J. Atmos. Sci.*, **54**, doi:10.1007/s13143-018-0030-2.

Kleist, D. T., 2011: Assimilation of tropical cyclone advisory minimum sea level pressure in the NCEP Global Data Assimilation System. *Wea. Forecasting*, **26**, 1085-1091, doi:10.1175/WAF-D-11-00045.1.

_____, and K. Ide, 2015: An OSSE-based evaluation of hybrid variational-ensemble data assimilation for the NCEP GFS. Part I: System description and 3D-hybrid results. *Mon. Wea. Rev.*, **143**, 433-451, doi:10.1175/MWR-D-13-00351.1.

Kwon, I.-H., S. English, W. Bell, R. Potthast, A. Collard, and B. Ruston, 2018: Assessment of progress and status of data assimilation in Numerical Weather Prediction. *Bull. Amer. Meteor. Soc.*, **99**, ES75-ES79, doi:10.1175/BAMS-D-17-0266.1.

Lazzara, M. A., R. Dworak, D. A. Santek, B. T. Hoover, C. S. Velden, and J. R. Key, 2014: High-latitude atmospheric motion vectors from composite satellite data. *J. Appl. Meteor. Climatol.*, **53**, 534-547, doi:10.1175/JAMC-D-13-0160.1.

Lee, M.-S., and D. M. Barker, 2005: Preliminary tests of first guess at appropriate time (FGAT) with WRF 3DVAR and WRF model. *J. Korean Meteor. Soc.*, **41**, 495-505.

Lorenc, A. C., 2003: The potential of the ensemble Kalman filter for NWP—a comparison with 4D-Var. *Quart. J. Roy. Meteor. Soc.*, **129**, 3183-3203, doi:10.1256/qj.02.132.

_____, N. E. Bowler, A. M. Clayton, S. R. Pring, and D. Fairbairn, 2015: Comparison of hybrid-4DEnVar and hybrid-4DVar data assimilation methods for global NWP. *Mon. Wea. Rev.*, **143**, 212-229, doi:10.1175/MWR-D-14-00195.1.

Marshall, A. G., and A. A. Scaife, 2009: Impact of the QBO on surface winter climate. *J. Geophys. Res.*, **114**, D18110, doi:10.1029/2009-JD011737.

Miyoshi, T., 2011: The Gaussian approach to adaptive covariance inflation and its implementation with the local ensemble transform Kalman filter. *Mon. Wea. Rev.*, **139**, 1519-1535, doi:10.1175/2010MWR3570.1.

Parlett, B. N., 1980: *The symmetric eigenvalue problem*, Prentice-Hall, 368 pp.

Parrish, D. F., and J. C. Derber, 1992: The National Meteorological Center's spectral statistical-interpolation analysis system. *Mon. Wea. Rev.*, **120**, 1747-1763

Penny, S. G., and T. M. Hamill, 2017: Coupled data assimilation for integrated earth system analysis and prediction. *Bull. Amer. Meteor. Soc.*, **98**, ES169-ES172.

Polavarapu, S., and M. Pulido, 2015: *Stratospheric and mesospheric data assimilation: The role of middle atmospheric dynamics. In Data Assimilation for Atmospheric, Oceanic and Hydrologic Applications (Vol. III),* Springer, 429-454.

Shin, S., J.-S. Kang, and Y. Jo, 2016: The local ensemble transform Kalman filter (LETKF) with a global NWP model on the cubed sphere. *Pure Appl. Geophys.*, **173**, 2555-2570, doi:10.1007/s00024-016-1269-0.

_____, and Coauthors, 2018: Real data assimilation using the Local Ensemble Transform Kalman Filter (LETKF) system for a global non-hydrostatic NWP model on the cubed-sphere (in press). *Asia-Pac. J. Atmos. Sci.*, **54**, doi: 10.1007/s13143-018-0022-2.

Song, H.-J., and I.-H. Kwon, 2015: Spectral transformation using a cubed-sphere grid for a three-dimensional variational data assimilation system. *Mon. Wea. Rev.*, **143**, 2581-2599, doi:10.1175/MWR-D-14-00089.1.

_____, G.-H. Lim, D.-I. LEE, and H.-S. Lee, 2009: Comparison of retrospective optimal interpolation with four-dimensional variational assimilation. *Tellus A*, **61**, 428-437.

_____, I.-H. Kwon, and J. Kim, 2017a: Characteristics of a spectral inverse of the Laplacian using spherical harmonic functions on a cubed-sphere grid for background error covariance modeling. *Mon. Wea. Rev.*, **145**, 307-322, doi:10.1175/MWR-D-16-0134.1.

_____, J. Kwun, I.-H. Kwon, J.-H. Ha, J.-H. Kang, S. Lee, H.-W. Chun, and S. Lim, 2017b: The impact of the nonlinear balance equation on a 3D-Var cycle during an Australian-winter month as compared with the regressed wind-mass balance. *Quart. J. Roy. Meteor. Soc.*, **143**, 2036-2049, doi:10.1002/qj.3036.

_____, S. Shin, J.-H. Ha, and S. Lim, 2017c: The advantages of hybrid 4DEnVar in the context of the forecast sensitivity to initial conditions. *J. Geophys. Res.* **122**, 12226-12244, doi:10.1002/2017JD027598.

_____, J.-H. Ha, I.-H. Kwon, J. Kim, and J. Kwun, 2018: Multi-resolution hybrid data assimilation core on a cubed-sphere grid (HybDA) (in press). *Asia-Pac. J. Atmos. Sci.*, **54**, doi:10.1007/s13143-018-0018-y.

Tripathi, O. P., and Coauthors, 2014: The predictability of the extratropical stratosphere on monthly time-scales and its impact on the skill of tropospheric forecasts. *Quart. J. Roy. Meteor. Soc.*, **141**, 987-1003, doi:10.1002/qj.2432.

Wu, W-S, R. J. Purser, D. F. Parrish, 2002: Three-dimensional variational analysis with spatially inhomogeneous covariances. *Mon. Wea. Rev,* **130**, 2905-2916, doi:10.1175/1520-0493(2002)130<2905:TDVAWS>2.0. CO;2.